Received ...; | Revised ...; | Accepted ...

DOI: xxx/xxxx

RESEARCH ARTICLE

Conductivity gain predictions for multiscale fibrous composites with interfacial thermal barrier resistance

Ernesto Iglesias-Rodríguez*[1] | Julián Bravo-Castillero[1] | Manuel E. Cruz[2]

[1]Unidad Académica del Instituto de Investigaciones en Matemáticas Aplicadas y en Sistemas en el Estado de Yucatán, Universidad Nacional Autónoma de México, Yucatán, Mexico

[2]Departamento de Engenharia Mecânica, Politécnica/COPPE, Universidade Federal de Rio de Janeiro, Rio do Janeiro - RJ, Brazil

Correspondence
*Corresponding author name, Email: ernesto.iglesias@iimas.unam.mx

Summary

Nanocomposites are heterogeneous media with two or more microstructural levels. For instance, a nano-level characterized by isolated nano-inclusions and a micro-level represented by the clusters resulting from aggregation processes. Our goal is to present a procedure to study the influence of this aggregation process and interfacial thermal resistance on the effective thermal conductivity. The procedure is based on the Reiterated Homogenization Method and consists of two stages. First, an effective intermediate thermal property is obtained by taking into account only the influence of the individual nano-inclusions in the matrix. Second, the final effective thermal coefficient ($\hat{k}_{RH}$) is calculated considering the clusters immersed in the intermediate effective medium derived in the first step. The conductivity gain (k_{gain}) is defined as the quotient ($\hat{k}_{RH}/\hat{k}_{CH}$) where $\hat{k}_{CH}$ is the effective thermal coefficient computed considering only one microstructural level. The scheme is exemplified for 2-D square arrays of circular cylinders. The analytical formulas of the effective coefficient used in the calculations generalize other well known formulas reported in the literature. Finally, the effect of thermal conductivity gain is illustrated as a function of the Biot number, the quotient of the thermal conductivities, the fibers volume fraction and an aggregation parameter. The present contribution could be useful for nano-reinforced fibers applications and nanofluids. Furthermore, the present formulas can be used to assess numerical computations. An appendix is included showing similarities and differences between the obtained analytical formulas of effective coefficients, for different truncation orders, and those derived from the trifasic model.

KEYWORDS:
conduction, reiterated homogenization, effective properties, imperfect contact, multiple scales

1 | INTRODUCTION

The study of the effective thermal conductivity in heterogeneous media with various micro-structural scales has gained increasing interest because of its importance in heat transfer applications, especially in the areas of nanocomposites[1,2,3,4,5] and nanofluids[6,7,8,9,10].

There is also an increasing interest in the influence of the thermal barriers at the interfaces[11,12]. In[13] an Ad-hoc homogenization model was developed to analyze the role of aggregation processes and interfacial thermal resistance on the effective thermal conductivity of nanofluids and nanocomposites. Based on the relationship between aggregation process and the existence of

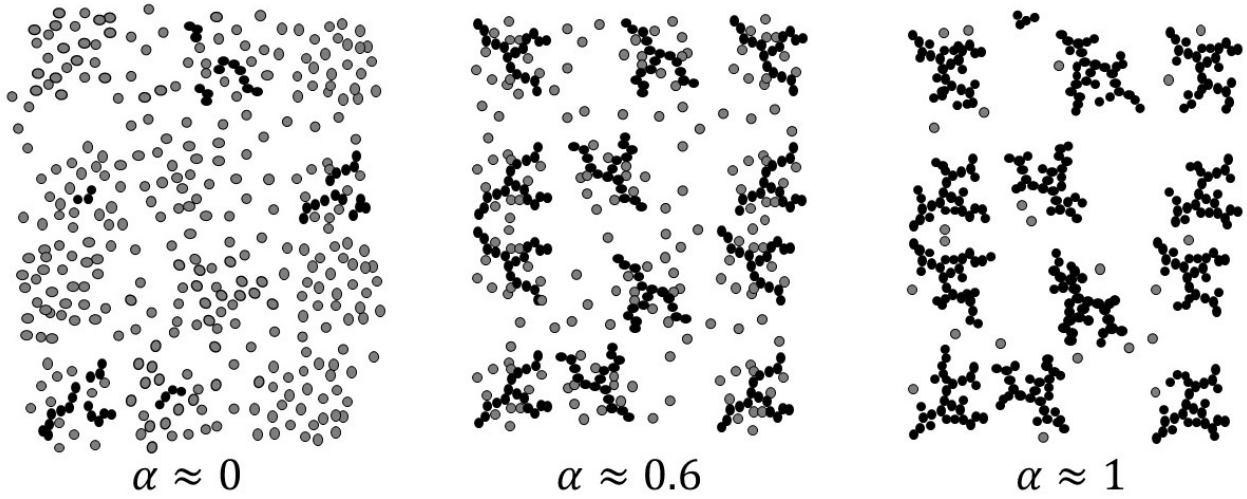

FIGURE 1 An illustration of the influence of aggregation in the base geometry (in black are marked the clustered inclusions).

multiple spatial scales, their model showed a significant enhancement of the effective thermal conductivity with respect to fully dispersed media.

The methodology to be followed in this work is based on the reiterated homogenization method (RH). This is a mathematical method of homogenization developed in [14]. The ad hoc multiscale model formulated by [13] was an inspiration for the application of RH in some of our works. For instance, in [15] the RH was applied to investigate the macroscopic behavior of the strong form Fourier heat conduction problem with periodic and rapidly oscillating coefficients depending on two fast variables representing two microstructural scales. Laminate composites were considered, and no improvement of the effective thermal conductivity was was observed relative to conventional laminates. However, in [16] perfect interfacial contact was considered and an improved effective thermal conductivity was observed for multiscale fibrous and particulate composites with-ordered microstructures by combining the reiterated homogenization method with known analytical formulas. Similar gain of the effective thermal conductivity was also observed in [17,18,19] for two-dimensional multiscale heterogeneous media through reiterated homogenization and finite element methods. In [12], a one-dimensional walk-through of the RH, involving numerical examples, mathematical justifications and examples of thermal conductivity gain can be seen. Recently, in [20], the methodology used in [15] was extended by considering the effects of thermal barriers at the interfaces, and also enhancement of the effective conductivity was detected.

In the current work, the analysis in [16] is generalized to the case of imperfect interfacial contact. For simplicity, we consider the same square periodic arrangement of circular cylinders for both microstructural levels. However, the formulas that we will use for the effective coefficients were calculated following the Rayleigh method described in [21,22,23]. Unlike [22,23], we derive in a conductive context five types of explicit analytical formulas for the effective thermal coefficient with different approximation orders. These formulas were obtained considering the imperfect spring-type contact condition at the interface [24]. Furthermore, these new formulas are expressed in the style of those reported by [25] for perfect contact in a three-phase conductive problem. In this way, the equivalence between the imperfect spring-type contact model with the three-phase model is detailed [26,24,27,28]. The validation also includes comparisons with finite element results and Laurent series expansion for small concentrations as in [29].

1.1 | Physical motivation

Let's consider a two-dimensional conductive medium formed from a matrix and inclusions with a periodic configuration. The inclusions in the nano-scale can be grouped into aggregates periodically distributed in the micro-scale. In this manner, we have two-scale periodic media where the bigger micro-structure is formed by a larger inclusion with the same conductivity as the smaller nano-structure.

To distinguish a medium which is fully aggregated, fully disperse or in an intermediate phase we will define an aggregation parameter (Figure 1). Following [13], for the described model we set

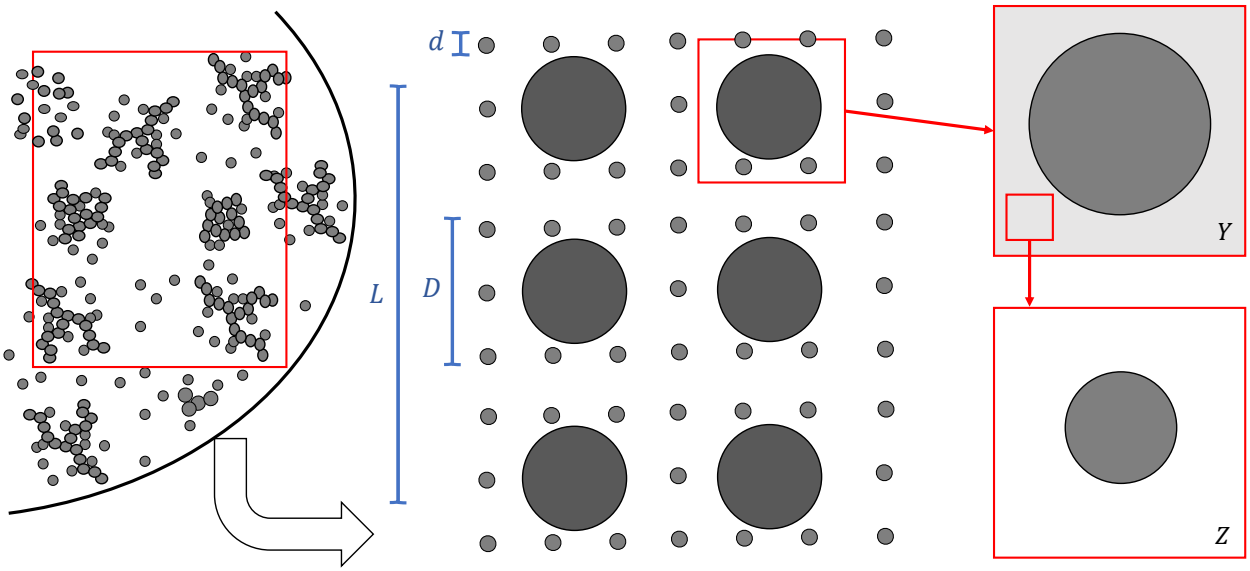

FIGURE 2 Schematic representation of a real material (left), proposed model (center) with-ordered microstructure and basic cells Y and Z (on the right). The d and D scales characterize the nano- and micro-level, respectively. The volume fraction in each basic cells depends on aggregation.

$$\alpha = \frac{\phi_c}{\phi} = \frac{\phi - \phi_{nc}}{\phi},$$

where ϕ is the volume fraction of the inclusions in the medium, ϕ_c is the volume fraction of the aggregates and ϕ_{nc} is the volume fraction of the inclusions that are not clustered in an aggregate ($\phi = \phi_c + \phi_{nc}$). In this way, when $\alpha = 0$ we have a fully disperse medium with only one scale formed by nano-scale inclusions in the matrix, and when $\alpha = 1$ we have a fully aggregated medium with one scale formed by micro-scale aggregates in the matrix.

For modeling purposes we will assume a periodic bimodal heterodisperse medium, that is, the inclusions have two different geometries and sizes (modes). The periods in each mode are assumed proportional, and then we will define the scales from the ratio between these periods. In this model, the largest inclusions would represent the clusters, for which we will consider the same conductivity as for an isolated particle, and which have managed to form a regular network. An example of this model is proposed in Figure 2 .

Aggregation relates directly with multiple spatial scales, and a significantly enhancement of the overall thermal conductivity was founded in media with multiple micro-scales, see, for instance,[13,1,3,16]. For both scales, we will consider a thermal barrier at the interfaces between matrix and inclusions, as will be described in the next section. Our interest is to compare media with multiple micro-scales against a single micro-scale, more details on this property gain will be given in section 4.

In the case of fibrous composite, we will only analyze fibers with circular cross-sections in the nanoscale. In the microscale, we consider clusters resulting from the aggregation process that will be represented as larger fibers with the same shape. A similar situation can be found in advanced composite material[30], for example, the addition of nanotubes to the matrix of fiber composites modifies their thermal and mechanical properties, even for low concentrations[31,32].

The paper continues as follows. In Section 2, we obtain the physical and mathematical formulation of the problem. Section 3, is devoted to the solving methodology, with special emphasis on reiterated homogenization and obtaining analytical formulas. More details on these formulas and a comparison with the triphasic model can be seen in the appendix. In Section 4, results on thermal conductivity gain will be given, in order to study the role of aggregation processes and interfacial thermal resistance in the effective coefficient. Finally, some concluding remarks are presented in Section 5.

2 | PROBLEM STATEMENT

We will model the heat conduction based on the Fourier heat equation in the interior of the body, and Dirichlet conditions on the boundaries (perfect thermal contact with the environment). We will also consider that there is an imperfect contact between the matrix and such inclusions, whether they are individual or clusters. That is assumed as a thermal barrier that induces a spring-type contact condition, i. e. the heat flow through each interface is proportional to the corresponding jump of temperature. The thermal barrier will be characterized by the non-dimensional Biot number[33,34,35]:

$$Bi = \frac{hS}{[\![K]\!]}, \tag{1}$$

that measures the thermal barrier at the interface with respect to the thermal conductivities of the components. Here $[\![K]\!]$ represents the jump in thermal conductivities, h is the interfacial conductance and S is the surface area of the contact. In this formulation, $Bi \to \infty$ indicates the presence of a perfect contact.

Here and henceforth we used the contrast notation $[\![(\cdot)]\!] = (\cdot)^{(m)} - (\cdot)^{(i)}$ where the indices indicates the expression being evaluated inside the domain representing an inclusion $(\cdot)^{(i)}$, or inside the domain representing the matrix $(\cdot)^{(m)}$. The next section will be devoted to the mathematical formulation of the heat transfer problem, for more details we refer to[20].

2.1 | Mathematical formulation

We will consider a conductive medium formed by a matrix and an arrangement of parallel fibers, assuming a periodic configuration. There is no loss of generality for this case if we consider the two-dimensional problem, that is, considering only a plane perpendicular to the fibers. These fibers can be grouped into clusters that will be considered individual fibers with arbitrary shape, assuming then that each fiber is in a single periodic cell. We will also consider that there is an imperfect contact between the matrix and such fibers, whether they are individual or clusters. We are interested in solving local problems in the principal directions (perpendicular to the directions of the fiber) and calculating the matrix of final effective properties.

For our study, we will consider only a uniaxially reinforced composite. This can be interpreted as a two-phase medium formed by a connected phase (matrix) and the non-connected phase formed by the repetition of the same domain (inclusions). These types of media are known as matrix-inclusion systems. We will assume a periodic arrangement of parallel cylindrical inclusions distributed evenly and periodically in a plane perpendicular to the axes of the cylinders.

Let the position of a typical point on the body be denoted by three coordinates (x_1, x_2, x_3) in a Cartesian coordinate system. We can assume, for example, that the axis x_3 corresponds to the transverse axis of symmetry in the direction of the cylindrical fiber. This means that the dimension of the problem is two and the cylinders are distributed in a periodic network of the transversal cross-section plane. In this sense, we will consider a domain $\Omega \subset \mathbb{R}^2$ with piecewise smooth boundaries $\partial\Omega$. Said domain extends over the spatial coordinate $x = (x_1, x_2) \in \mathbb{R}^2$ (known as a slow variable) and cylinders reduce to circles.

In this context, we will consider a complex structure that can be periodically characterized by two microstructural levels. A first level with period D and a second level with period d. In this way, for a medium with characteristic length L we can consider the small parameters:

$$\varepsilon_1 = \frac{D}{L}, \qquad \varepsilon_2 = \frac{d}{L},$$

where $\varepsilon_1 \ll 1$ (the parameter is small) and $\varepsilon_2 \ll \varepsilon_1$ (there is a clear scales separation)[36,37]. For simplicity we will consider $\varepsilon_1 = \varepsilon$ and $\varepsilon_2 = \varepsilon^2$ (i. e. the case $d = \varepsilon D$).

The presence of two micro-structural periodic scales is related to the existence of two periodic cells εY, $\varepsilon^2 Z$ whose repeated application covers the domain Ω[20,4]. We will consider unitary squares for these cells

$$\left(-\frac{1}{2}, \frac{1}{2}\right) \times \left(-\frac{1}{2}, \frac{1}{2}\right),$$

and restrict our study to a periodic conductive composite with two components with known behavior (two-phase), although the extension to other multiphase media is direct. This means that each cell is formed by non-empty subsets[38,39],

$$\begin{aligned} Y &= Y^{(m)} \cup Y^{(i)} \quad (\partial Y^{(i)} \cap \partial Y = \emptyset), \\ Z &= Z^{(m)} \cup Z^{(i)} \quad (\partial Z^{(i)} \cap \partial Z = \emptyset), \end{aligned} \tag{2}$$

where $Y^{(i)}$ and $Z^{(i)}$ represent the region occupied by the inclusions at each scale. For the model defined in Section 1.1 we denote by $K^{(m)}$ and $K^{(i)}$ the thermal conductivities of matrix and inclusions, respectively. Notice that the volume fractions can

be expressed as

$$\phi_c = \frac{|Y^{(i)}|}{|Y|} = |Y^{(i)}|, \qquad \phi_{nc} = (1-\phi_c)\frac{|Z^{(i)}|}{|Z|} = (1-\phi_c)|Z^{(i)}|,$$

where $|\omega| = \int_\omega dV$.

We will consider the steady-state ε-dependent multiscale heat conduction boundary value problem[20]; i. e.

Global Problem: *find* $u^\varepsilon \in C^2(\Omega \setminus \Gamma^\varepsilon)$, *such as*

$$L^\varepsilon u^\varepsilon \equiv -\nabla \cdot (K^\varepsilon \nabla u^\varepsilon) = f \qquad \text{in } \Omega \setminus \Gamma^\varepsilon, \tag{3}$$

$$K^\varepsilon \nabla u^\varepsilon \cdot n = -B^\varepsilon [\![u^\varepsilon]\!] \qquad \text{on } \Gamma^\varepsilon = \Gamma_Y^\varepsilon \cup \Gamma_Z^\varepsilon, \tag{4}$$

$$[\![K^\varepsilon \nabla u^\varepsilon \cdot n]\!] = 0 \qquad \text{on } \Gamma^\varepsilon = \Gamma_Y^\varepsilon \cup \Gamma_Z^\varepsilon, \tag{5}$$

$$u^\varepsilon = 0 \qquad \text{on } \partial\Omega, \tag{6}$$

where $K^\varepsilon = K(x/\varepsilon, x/\varepsilon^2)$ and f are the thermal conductivity and heat output, respectively. In these equations x represents the spatial variable on a global scale and

$$B^\varepsilon = \begin{cases} \beta\varepsilon^{-1}, \text{ on } \Gamma_Y^\varepsilon \\ \beta\varepsilon^{-2}, \text{ on } \Gamma_Z^\varepsilon \end{cases}$$

is the Biot number[33,35]. The thermal conductivity tensor K^ε is symmetric, positive definite, and it is worth noting that for small ε its coefficients are rapidly oscillating.

Now we are going to present the fundamental theory which allows us to pass from problem (3)-(6) to an equivalent (homogenized) one whose coefficients are constant. This constant coefficient is known as the effective coefficient of the macro-scale or *global effective coefficient*, and will be obtained in the next section (equation (12)). The derived problem will be solved using the theory of complex variable functions and will present various estimates of the effective coefficients.

3 | ASYMPTOTIC HOMOGENIZATION METHOD

Homogenization is an upscaling procedure that provides mathematical models that allow the calculations of effective properties of a composite from known properties of its components. In this manner, the macroscopic behavior of a heterogeneous medium is obtained as an equivalent homogeneous material based on the relationships at the smallest scales.

From the mathematical point of view, the homogenization process transforms problems involving systems of partial differential equations with rapidly oscillating coefficients in a homogenized problem with constant ones, called effective coefficients. In a previous work[20], the formal procedure to derive the homogenized problem and effective coefficients are described for a general three-dimensional problem. The solution of local problems in each micro-structural scale is used to calculate the effective coefficients. This is the case for the model defined in Section 1.1, when the aggregation parameter $\alpha \in \{0, 1\}$.

The name homogenization was introduced in[40,41,42], who worked a similar approach to the prior work of[43]. Since then there have been great advances in this theory and it has proven to be very useful in all kinds of applications. For our work we use the Asymptotic Homogenization Method (A.H.M), which was stated by[14,44,45] and systematically formalized to handle homogenization of contour problems with rapidly oscillating periodic coefficients[46,47]. This is based on the asymptotic expansion of the solution of the boundary problem, and the idea is to obtain a homogenized problem whose solution u_0 is the limit (when $\varepsilon \to 0$) of the solutions u^ε of (3)-(6).

3.1 | Reiterated homogenization

The Reiterated Homogenization Method (RHM) is a rigorous mathematical technique for investigating the macroscopic behavior of periodic composites with different micro-structural levels[14]. In our case, and due to the presence of multiple scales, we will apply this formalism in the context of the reiterated homogenization. More details on this procedure can be found in[20], but it can be stated briefly as follow.

An asymptotic expansion for the solution with the form

$$u(x, y, z) = u_0(x) + \varepsilon u_1(x, y) + \varepsilon^2 u_2(x, y, z) + O(\varepsilon^3) \tag{7}$$

will be proposed, where each u_i is considered Y-periodic respect to $y = x/\varepsilon$ and Z-periodic respect to $z = x/\varepsilon^2$ (these new variables are known as fast variables).

Formally applying the operators in (3)-(5) to the series described, and after some manipulations, we obtain a recurring chain of problems whose solutions are the coefficients of (7). In particular, u_0 is the solution to the next problem

Homogenized Problem: *find* $u \in C^2(\Omega)$, *such as*

$$-\nabla \cdot (\hat{K}\nabla u_0) = f \qquad \text{in } \Omega, \tag{8}$$

$$u_0 = 0 \qquad \text{on } \partial\Omega, \tag{9}$$

where the $\hat{K}$ is the *global effective coefficients* for the macro-scale. This is a symmetric, positive definite, constant tensor, in contrast with K^ϵ which is rapidly oscillating.

In terms of the proposed model (section 1.1) we consider, in the nano-scale,

$$K(y,z) = \begin{cases} K^{(m)}, & z \in Z^{(m)}, y \in Y^{(m)} \quad \text{(i.e. matrix)}, \\ K^{(i)}, & z \in Z^{(i)}, y \in Y^{(m)} \quad \text{(i.e. isolated inclusion)}, \\ K^{(i)}, & y \in Y^{(i)} \quad \text{(i.e. aggregates)}. \end{cases} \tag{10}$$

We will consider the same conductivity for the aggregates as for an isolated inclusion, and they are represented as larger inclusions in the micro-scale with the form

$$\bar{K}(y) = \begin{cases} K^1, & y \in Y^{(m)} \quad \text{(i.e. effective matrix)}, \\ K^{(i)}, & y \in Y^{(i)} \quad \text{(i.e. aggregates)}. \end{cases} \tag{11}$$

We find $\hat{K}$ in the form

$$\hat{k}_{ij} = \left\langle \bar{k}_{ij} - \bar{k}_{ik}\frac{\partial N_j}{\partial y_k} \right\rangle_Y, \tag{12}$$

but $\bar{K}(y)$ depends on the micro-scale through K^1. This *intermediate effective coefficient* have the form

$$k^1_{ij} = \left\langle k_{ij} - k_{ik}\frac{\partial N^y_j}{\partial z_k} \right\rangle_Z. \tag{13}$$

The given formulas for both effective coefficients $(K^1, \hat{K})$ are depending on functions (N^y_j, N_j) that will be obtained as solutions of what are known in A.H.M as *local problems*.

Local Problem 1: *find the family* $\{N^y_j\}_{y\in Y}$ Z*-periodic such as*

$$-\nabla_z \cdot \left(K - K\nabla_z N^y_j\right) = 0, \qquad \text{in } Z \setminus \Gamma_Z, \tag{14}$$

$$K - K\nabla_z N^y_j = -B[\![N^y_j]\!], \qquad \text{on } \Gamma_Z, \tag{15}$$

$$[\![K - K\nabla_z N^y_j]\!] = 0, \qquad \text{on } \Gamma_Z, \tag{16}$$

$$\left\langle N^y_j \right\rangle_Z = 0. \tag{17}$$

Local Problem 2: *find* N_j Y*-periodic such as*

$$\nabla_y \cdot \left(\bar{K} - \bar{K}\nabla_y N_j\right) = 0, \qquad \text{in } Y \setminus \Gamma_Y, \tag{18}$$

$$\bar{K} - \bar{K}\nabla_y N_j = -B[\![N_j]\!], \qquad \text{on } \Gamma_Y, \tag{19}$$

$$[\![\bar{K} - \bar{K}\nabla_y N_j]\!] = 0, \qquad \text{on } \Gamma_Y, \tag{20}$$

$$\left\langle N_j \right\rangle_Z = 0. \tag{21}$$

It is worth noting that a single microstructural scale (conventional homogenization)[48,45,49] become special cases of the more general treatment presented here. We will consider both single microstructural scale and later we will extend these results to the case of two microstructural scales.

Our final goal is to analyze the role of aggregation processes (single scale against multiple scales) and interfacial thermal resistance in the effective thermal conductivity. The results of this comparison will be given in section 4.

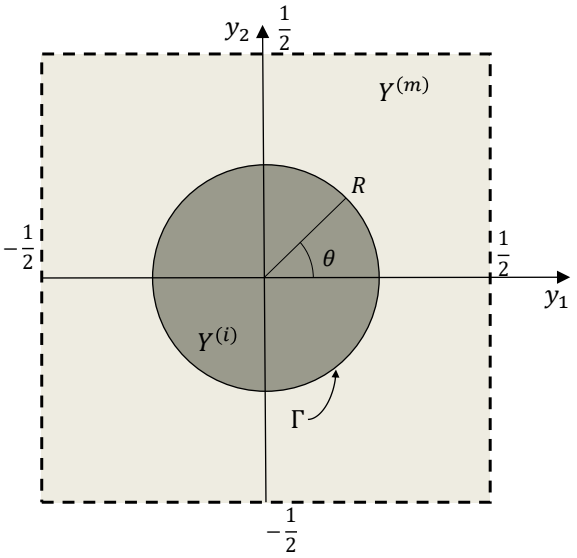

FIGURE 3 Square periodic cell with circular inclusion.

The previous development is valid for any geometry, number of dimensions and any material[20]. We will solve this problem in the case of homogeneous isotropic components, inclusion with circular cross section and assuming constant conductance at the interface.

3.2 | Analytical solution of the local problems

The geometric arrangement described in 2.1 is equivalent, in the complex plane, to the structures known as *lattices*[46,50]. We will use the theory of complex variable functions to solve the local problem in the isotropic case. We will follow the methodology proposed by[22] although the notations and development follow the works of[21,51,52].

As we are solving the problem for homogeneous isotropic materials, we will denote by $W = Y, Z$ and by

$$\mathcal{K} = (\kappa(\xi)\delta_{ij}),$$

where $\mathcal{K} = K, \bar{K}, \xi = y, z$, and

$$\kappa(\xi) = \begin{cases} \kappa^{(m)}, & \xi \in W^{(m)} \qquad \text{i.e. (in the matrix)}, \\ \kappa^{(i)}, & \xi \in W^{(i)} \qquad \text{i.e. (in the inclusion)}. \end{cases}$$

We assumed here that $\kappa^{(i)} \neq 0$, the case of empty fibers (perforated material) is extensible analyzed in[53,54,52].

By isotropy, (14) and (18) are equivalent to Laplace's equation and N_k are harmonic functions. Under this conditions the problems in question have the form:

Find N_k, $W-$*periodic such as*

$$\nabla^2 N_k = 0, \qquad \text{in } W \setminus \Gamma \tag{22}$$

$$-[\![\kappa \frac{\partial N_k}{\partial \xi_i}]\!]\eta_i = [\![\kappa]\!]\eta_k \qquad \text{on } \Gamma \tag{23}$$

$$-\kappa \frac{\partial N_k}{\partial \xi_i}\eta_i = \kappa\eta_k - \beta[\![N_k]\!]. \qquad \text{on } \Gamma \tag{24}$$

Although we will only solve this problem below for $k = 1$, the case $k = 2$ is analogous.

We will consider that each inclusion is *centered* at the origin of coordinates of the periodic cell, in the sense that said point belongs to the domain represented by the inclusion (Fig. 3). We will denote then by

$$\xi_1 = \mathcal{R}e(z), \qquad \xi_2 = \mathcal{I}m(z).$$

The inclusions are located in a network of the plane generated by a pair of vectors $\omega_1, \omega_2 \in \mathbb{C}$ such as $\mathcal{I}m(\omega_2/\omega_1) \neq 0$. Double periodic harmonic functions are sought in the regions formed by the matrix ($Y^{(m)}$) and the inclusion ($Y^{(i)}$) for each local problem. We also know that there must be some analytical function in the complex plane $\Phi(z)$ such as

$$N_1 = \mathcal{R}e\left\{\Phi(z)\right\}, \tag{25}$$

and $\mathcal{I}m\left\{\Phi(z)\right\}$ is its conjugate harmonic[50]. We will propose solutions of the form

$$\Phi(z) = \begin{cases} \Phi_{in} = \displaystyle\sum_{n=0}^{\infty} c_{2n+1} z^{2n+1}, & z \in Y^{(i)} \quad \text{(inclusion)}, \\ \Phi_{ex} = a_0 z + \displaystyle\sum_{n=0}^{\infty} \frac{a_{2n+1}}{(2n)!} \frac{d^{2n}\zeta}{dz^{2n}}(z), & z \in Y^{(m)} \quad \text{(matrix)}. \end{cases} \tag{26}$$

where $\zeta(z) = \zeta(z, \omega_1, \omega_2)$ is the Weierstrass Zeta[55] function and the coefficients a_i, c_i are reals.

The term

$$a_0 = \frac{\delta_1}{\omega_1} a_1$$

is obtained from the periodicity condition from the Legendre relation[55]:

$$\delta_1 \omega_2 - \delta_2 \omega_1 = 2\pi i.$$

The remaining indeterminate coefficients a_k and c_k will be obtained from evaluating the proposal (26) formally in the contact conditions (23)-(24). For this, we will use Laurent's series development, which is of the form[21,56]:

$$\Phi_{ex} = \sum_{n=0}^{\infty} \left(a_{2n+1} z^{-2n-1} + \sigma_{2n+1} z^{2n+1} \right), \tag{27}$$

where

$$\sigma_l = \sum_{k=1}^{\infty}{}^{o} a_k \eta_{kl} \equiv \sum_{n=0}^{\infty} a_{2n+1} \eta_{2n+1\, l}, \tag{28}$$

$$\eta_{11} = \frac{\delta_1}{\omega_1}, \tag{29}$$

$$\eta_{kl} = -\frac{(k+l-1)!}{(k-1)!l!} S_{k+l} = -\left(\!\!\binom{k}{l}\!\!\right) S_{k+l}, \quad (k+l>2), \tag{30}$$

$$S_\lambda = \sum_{m^2+n^2 \neq 0} \left(m\omega_1 + n\omega_2 \right)^{-\lambda}, \quad (\lambda > 2). \tag{31}$$

We have used here the notation $\sum^o$ to indicate that the sum is carried out only on the odd index. $\left(\!\binom{k}{l}\!\right)$ is known as the multiset number[57] and is related to the generalization of combinatorial numbers[58]. The sums S_λ are known as lattice sum.

For the case of a circular cross section and constant conductance at the interface (Fig. 3), we can parameterize the boundary in such a way that

$$\Gamma = \left\{ z = Re^{i\theta} \,:\, R = \text{constante} \in \left(0, \frac{1}{2}\right), \qquad -\pi \leq \theta \leq \pi \right\}.$$

Note also that, on Γ, $\eta = (\eta_1, \eta_2) = (\cos\theta, \sin\theta) = \frac{1}{R}\left(\frac{d\xi_2}{d\theta}, -\frac{d\xi_1}{d\theta}\right)$.

Substituting the series (26),(27) in (23),(24), and by the Cauchy-Riemann relations, the following equations written in the form of expansion in cosine series are obtained:

$$\sum_{k=1}^{\infty}{}^{o} \Big(\kappa^{(m)}[-a_k R^{-2k} + \sigma_k] - \kappa^{(i)} c_k + (\kappa^{(m)} - \kappa^{(i)}) \delta_{1k} \Big) k R^k \cos(k\theta) = 0, \tag{32}$$

$$\kappa^{(i)} \sum_{k=1}^{\infty}{}^{o} (c_k + \delta_{1k}) k R^k \cos(k\theta) = \beta \sum_{k=1}^{\infty}{}^{o} \left(-c_k + a_k R^{-2k} + \sigma_k \right) R^k \cos(k\theta). \tag{33}$$

Using here the orthogonality of $\{\cos(k\theta)\}_k$ as square-integrable functions we have

$$\frac{\kappa^{(i)}}{\kappa^{(m)}} c_k = -a_k R^{-2k} + \sigma_k + (1-\rho)\delta_{1k}, \tag{34}$$

$$c_k = \beta(\beta + \kappa^{(i)} k)^{-1} \left(a_k R^{-2k} + \sigma_k - \frac{\kappa^{(i)}}{\beta} \delta_{1k} \right). \tag{35}$$

Note that to use the orthogonality as square-integrable functions we require that the series formed by the sum of the squares of the coefficients multiplying $\cos(k\theta)$ to be convergent. For this, it is sufficient to consider the bounding of $\{a_k\}_k$ and $\{c_k\}_k$.

Finaly equating the coefficients c_k in (34) and (35) we obtain the following infinite linear system of equations:

$$\beta_k \left(\sum_{n=0}^{\infty} a_{2n+1} \eta_{2n+1\ k} + \delta_{1k} \right) - a_k R^{-2k} = 0. \tag{36}$$

where k are odd and

$$\beta_k = \frac{(1-\rho)\beta + \kappa^{(i)} k}{(1+\rho)\beta + \kappa^{(i)} k} \qquad \left(\rho = \frac{\kappa^{(i)}}{\kappa^{(m)}} \right). \tag{37}$$

This result agree with those obtained in[22,56] for elastic media. When $\beta \to \infty$:

$$\lim_{\beta \to \infty} \beta_k = \frac{1-\rho}{1+\rho} = \frac{\kappa^{(m)} - \kappa^{(i)}}{\kappa^{(m)} + \kappa^{(i)}},$$

and our formulation coincide with those reported in[51,21].

Additionally, it is convenient, in some contexts, to write the system (36) in its matrix form. Let us denote the following infinite matrices by

$$I = (\delta_{kl}), \qquad H = (\eta_{kl}), \qquad P = (\delta_{kl} R^k), \qquad B = (\delta_{kl} \beta_k).$$

With this notation, the vectors being infinite $a = (a_1, a_3, \dots)^\top$ and $e_1 \equiv (1, 0, 0, \dots)^\top$, the system can be written as

$$Ma \equiv (I - BP^2 H)a = v, \tag{38}$$

where $v = BP^2 e_1 = (\beta_1 R^2, 0, 0, \dots)^\top$ and $BP^2 H = (\beta_k R^{2k} \eta_{kl})$.

3.3 | Effective coefficient aproximations

In this section, we will obtain approximations to the solutions of the infinite system and the effective coefficients associated with these approximations through finite order truncations.

To calculate the effective properties (12) and (13) we can use

$$\begin{aligned} \hat{\kappa}_{ij} &= \left\langle \kappa_{ij} \right\rangle_W + \left\langle \kappa_{ik} \frac{\partial N_j}{\partial y_k} \right\rangle_W \\ &= \delta_{ij} \left\langle \kappa \right\rangle_W + \left\langle \kappa \frac{\partial N_j}{\partial y_i} \right\rangle_W . \end{aligned} \tag{39}$$

For κ_{11} we can apply the Green theorem to get

$$\begin{aligned} \left\langle \kappa \frac{\partial N_1}{\partial y_1} \right\rangle_W = -\int_{-\pi}^{\pi} \sum_{k=1}^{\infty}{}^{o} \Big(& \kappa^{(m)} \left[a_1 \eta_{11} \delta_{1k} + a_k R^{-2k} + \sigma_k \right] \\ & - \kappa^{(m)} \left[a_1 \eta_{11} \delta_{1k} - a_k R^{-2k} + \sigma_k + (1-\rho)\delta_{1k} \right] \Big) \\ & R^k \cos(k\theta) R \cos\theta \, d\theta \\ = -\sum_{k=1}^{\infty}{}^{o} \kappa^{(m)} & \left[2 a_k R^{-2k} - (1-\rho)\delta_{1k} \right] R^{k+1} \int_{-\pi}^{\pi} \cos(k\theta) \cos\theta \, d\theta, \end{aligned}$$

and $\int_{-\pi}^{\pi} \cos(k\theta)\cos\theta d\theta = \pi\delta_{k1}$. It is obtained then

$$\begin{aligned}\hat{\kappa}_{11} &= \kappa^{(m)} - (\kappa^{(m)} - \kappa^{(i)})\pi R^2 + (\kappa^{(m)} - \kappa^{(i)})\pi R^2 - 2\kappa^{(m)}\pi a_1 \\ &= \kappa^{(m)}(1 - 2\pi a_1).\end{aligned} \tag{40}$$

For the rest of coefficients

$$\hat{\kappa}_{12} = \hat{\kappa}_{21} = 0, \tag{41}$$

$$\hat{\kappa}_{22} = \hat{\kappa}_{11}, \tag{42}$$

This means that it is not necessary to solve the entire infinite system but only to find the solution for the first variable a_1. For small order truncations it is possible to find formulas where few terms are involved, however, for the rest of truncations it is convenient to use the system in its matrix form (38) and solve it by numerical methods.

Take for example a **first-order** truncation of the system (36). That is, when we keep only a single unknown (a_1) in (36). Then

$$\beta_1\Big[a_1\eta_{11} + 1\Big] - a_1 R^{-2} = 0, \tag{43}$$

Thus

$$a_1 = -\beta_1(\beta_1\eta_{11} - R^{-2})^{-1} = (R^{-2}\beta_1^{-1} - \eta_{11})^{-1}, \tag{44}$$

where

$$\beta_1 = \frac{(1-\rho)\beta + \kappa^{(i)}}{(1+\rho)\beta + \kappa^{(i)}}.$$

For the square cell, from (40) it is obtained

$$\frac{\hat{\kappa}_{11}}{\kappa^{(m)}} = \frac{1 - \pi R^2\beta_1}{1 + \pi R^2\beta_1} = \frac{1 - \phi\beta_1}{1 + \phi\beta_1}. \tag{45}$$

This result agrees with the classic results of[59,60], who derive them independently for a spheroid of which the fiber is the limiting case when its major axis tends to infinity. Equivalent formulas were obtained by[61,51,21] in the perfect contact case ($\beta \to \infty$). Also of interest are the cases $\kappa^{(i)} \in \{0, \infty\}$:

$$\lim_{\kappa^{(i)}\to 0}\frac{\hat{\kappa}_{11}}{\kappa^{(m)}} = \frac{1-\phi}{1+\phi} \qquad \lim_{\kappa^{(i)}\to \infty}\frac{\hat{\kappa}_{11}}{\kappa^{(m)}} = \frac{1+\phi}{1-\phi}.$$

These limit cases correspond to media whose inclusions are thermally insulating or superconductive, respectively, and agree with classic results.

In the case of a **second-order** truncation of the system (36) we have:

$$\beta_1\Big[a_1\eta_{11} + a_3\eta_{31} + 1\Big] - a_1 R^{-2} = 0, \tag{46}$$

$$\beta_3\Big[a_1\eta_{13} + a_3\eta_{33}\Big] - a_3 R^{-6} = 0. \tag{47}$$

We shall notice that, for a square cell $\eta_{11} = -\pi, \eta_{31} = -3S_4, \eta_{13} = -S_4$ and $\eta_{33} = 0$, where

$$S_4 = \frac{\Gamma\left(\frac{1}{4}\right)^8}{960\pi^2} \approx 3.1512120021538975\ldots$$

Finally, by Cramer's rule, we get

$$\frac{\hat{\kappa}_{11}}{\kappa^{(m)}} = \frac{1 - \phi\beta_1 - 3S_4^2\pi^{-4}\beta_1\beta_3\phi^4}{1 + \phi\beta_1 - 3S_4^2\pi^{-4}\beta_1\beta_3\phi^4}. \tag{48}$$

Similarly, for a **third-order** truncation we obtain:

$$\frac{\hat{\kappa}_{11}}{\kappa^{(m)}} = \frac{1 - \phi\beta_1 - 3S_4^2\pi^{-4}\beta_1\beta_3\phi^4/\Delta_1}{1 + \phi\beta_1 - 3S_4^2\pi^{-4}\beta_1\beta_3\phi^4/\Delta_1}, \tag{49}$$

where

$$\Delta_1 = 1 - 735S_8^2\pi^{-8}\beta_3\beta_5\phi^8, \tag{50}$$

and

$$S_8 = \frac{3}{7}S_4^2 \approx 4.2557730353651895\ldots$$

TABLE 1 Comparison of effective conductivities in the case of thermally insulating fibers ($\rho = 10^{-6}/3$) for different approximations and known results

ϕ	Eq.(45)	Eq.(48)	Eq.(49)	Eq.(51)	[25]*	[22]**	[62]†
0.1	0.818182	0.818177	0.818177	0.818177	0.818177	0.818177	0.818177
0.2	0.666667	0.666531	0.666531	0.666531	0.666531	0.666530	0.666530
0.3	0.538462	0.537580	0.537580	0.537580	0.537580	0.537580	0.537580
0.4	0.428572	0.425358	0.425355	0.425351	0.425351	0.425350	0.425350
0.5	0.333333	0.324729	0.324681	0.324655	0.324655	0.324654	0.324653
0.6	0.25	0.230949	0.230477	0.230329	0.230322	0.230318	0.23032

* Table 1, 6th order formula, at [25]

** Table 3, at [22]

† Table 7, at [62]

Furthermore, a **fourth-order** truncation leads to the following formula:

$$\frac{\hat{\kappa}_{11}}{\kappa^{(m)}} = \frac{1 - \phi\beta_1 - C_4\beta_1\beta_3\phi^4/\Delta_2 - C_8\beta_1\beta_7\phi^8\Delta_1'/\Delta_2}{1 + \phi\beta_1 - C_4\beta_1\beta_3\phi^4/\Delta_2 - C_8\beta_1\beta_7\phi^8\Delta_1'/\Delta_2}, \tag{51}$$

where

$$\begin{aligned} C_4 &= 3S_4^2\pi^{-4}, \quad C_8 = 7S_8^2\pi^{-8}, \\ \Delta_1'(\phi) &= \Delta_1(\phi) - b_{12}\beta_5\beta_7\phi^{12}, \\ \Delta_2 &= 1 - 735S_8^2\pi^{-8}\beta_3\beta_5\phi^8 - 66^2\cdot 35S_{12}^2\pi^{-12}\beta_5\beta_7\phi^{12}, \end{aligned}$$

and

$$S_{12} = \frac{18}{143}S_4^3 \approx 3.9388490128279704\ldots$$

The fourth-order formula (51) will be used in section 4 to obtain the effective coefficient via conventional and reiterated homogenization. As a matter of validation, we compare next our approach with analytical formulas, variational bounds, numerical results, and limiting cases found in the literature.

Higher-order formulas can be found from this procedure, but the current ones are sufficient for our goal. The obtained formulas of the fifth order have the form

$$\frac{\hat{\kappa}_{11}}{\kappa^{(m)}} = \frac{1 - \phi\beta_1 - C_4\beta_1\beta_3\phi^4\Delta_0(\phi)/\Delta_3(\phi) - C_8\beta_1\beta_7\phi^8\Delta_2'(\phi)/\Delta_3(\phi)}{1 + \phi\beta_1 - C_4\beta_1\beta_3\phi^4\Delta_0(\phi)/\Delta_3(\phi) - C_8\beta_1\beta_7\phi^8\Delta_2'(\phi)/\Delta_3(\phi)}. \tag{52}$$

For detailed information of these functions we refer to table 5 of the appendix.

3.4 | Validation

As mentioned in section 3.2, the system (36) agree with the ones presented by [22,56]. In this section we will evaluate the behavior of the different proposed truncations, comparing them with the results obtained there and others present in the literature.

Similar developments to ours are found in the literature for elastic materials. In the table 1 it is compared with the effective longitudinal shear modulus for a lattice of square cells and thermally insulating fibers (voids in the elastic equivalent). In this case, even second formulas are very accurate comparing them with the results present in the literature, and small improvement are obtained from higher order.

In tables 2 and 3 the effective conductivities obtained for an arrangement of square cells with our approximations are shown, comparing them with results present in the literature [25,22,33]. We have considered $\phi = 0.3$ and $\phi = 0.75$ as representative of the small and large volume fractions, respectively. For small values of the volume fraction, all approximations are very similar. Even first-order formulas result in very accurate results for small concentrations, as we will see next from Laurent series analysis. For high volume fraction the difference is more notable with increasing ρ. This difference should vanish for higher order truncations, as seen in table 4 near percolation. In this case, the numerical solution given by [23] for $N_0 = 0, 1, 2, 3$ are equivalent to Eq.(45), (48), (49) and Eq.(51), respectively.

TABLE 2 Comparison of effective conductivities in the case of low volume fraction ($\phi = 0.3$) for different approximations and known results

Bi	ρ	Eq.(45)	Eq.(48)	Eq.(49)	Eq.(51)	[25]*	[22]**	[33]†
10^{-7}		0.538462	0.537580	0.537580	0.537580	0.537580	0.537580	0.537620
10^{-5}		0.538465	0.537584	0.537584	0.537584	0.537584	0.537584	0.537620
0.001		0.538816	0.537937	0.537937	0.537936	0.537936	0.537936	0.537970
0.01		0.541993	0.541129	0.541129	0.541128	0.541128	0.541128	0.541170
0.1		0.572212	0.571480	0.571480	0.571479	0.571479	0.571479	0.571510
1	2	0.772152	0.771995	0.771995	0.771995	0.771995	0.771995	0.772020
10		1.111801	1.111799	1.111799	1.111799	1.111799	1.111800	1.111800
100		1.209302	1.209353	1.209353	1.209353	1.209353	1.209350	1.209300
1000		1.220908	1.220974	1.220974	1.220974	1.220974	1.220970	1.220900
10^5		1.222209	1.222277	1.222277	1.222277	1.222277	1.222280	1.222200
10^7		1.222222	1.222290	1.222290	1.222290	1.222290	1.222290	1.222300
10^{-7}		0.538462	0.537580	0.537580	0.537580	0.537580	0.537580	0.537620
10^{-5}		0.538465	0.537584	0.537584	0.537584	0.537584	0.537584	0.537620
0.001		0.538816	0.537937	0.537937	0.537936	0.537936	0.537936	0.537970
0.01		0.541993	0.541129	0.541129	0.541128	0.541128	0.541128	0.541170
0.1		0.572212	0.571480	0.571480	0.571479	0.571479	0.571479	0.571510
1	50	0.772152	0.771995	0.771995	0.771995	0.771995	0.771995	0.772020
10		1.111801	1.111799	1.111799	1.111799	1.111799	1.111800	1.111800
100		1.209302	1.209353	1.209353	1.209353	1.209353	1.209350	1.209300
1000		1.220908	1.220974	1.220974	1.220974	1.220974	1.220970	1.220900
10^5		1.222209	1.222277	1.222277	1.222277	1.222277	1.222280	1.222200
10^7		1.222222	1.222290	1.222290	1.222290	1.222290	1.222290	1.222300

* Table 1, 6th order formula, at [25]

** Table 3, at [22]

† Table 1, at [33]

To analyze the approximation orders obtained in (45), (48), (49) and (51) it is necessary to write the developments in Laurent series around $\phi = 0$. For example, in the case of (45):

$$\frac{1-\phi\beta_1}{1+\phi\beta_1} = 1 + 2\sum_{j=1}^{\infty}\left(-\beta_1\phi\right)^j. \tag{53}$$

The complexity of these developments increases as the truncation is of a higher order. However, we were able to obtain an expression up to the eighth term, which is true for all higher-order truncations. Moreover the Laurent series of (51) and those of the highest order formulas proposed by [25] (see table 5 of the appendix) coincide up to the twelfth term, and have the form:

$$\begin{aligned}\frac{\hat{\kappa}_{11}}{\kappa^{(m)}} = 1 &+ 2\sum_{j=1}^{12}\left(-\beta_1\right)^j\phi^j - 2\sum_{j=1}^{8}\left(3jS_4^2\pi^{-4}\left(-\beta_1\right)^{j+1}\beta_3\right)\phi^{4+j} \\ &+ 2\sum_{j=1}^{4}\left(9\frac{j(j+1)}{2}S_4^4\pi^{-8}\left(-\beta_1\right)^{j+2}\beta_3^2 - 7jS_8^2\pi^{-8}\left(-\beta_1\right)^{j+1}\beta_7\right)\phi^{8+j} \\ &+ O(\phi^{13}).\end{aligned} \tag{54}$$

The development (54) is a generalization of [29, Eq. 76], and coincides exactly with it in the context of perfect contact, i.e. when $\beta \to \infty$.

TABLE 3 Comparison of effective conductivities in the case of high volume fraction ($\phi = 0.75$) for different approximations and known results

Bi	ρ	Eq.(45)	Eq.(48)	Eq.(49)	Eq.(51)	[25]*	[22]**	FEM [33]†
10^{-7}		0.142857	0.092688	0.083926	0.080420	0.080038	0.078424	0.078423
10^{-5}		0.142862	0.092693	0.083932	0.080426	0.080044	0.078431	0.078438
0.001		0.143347	0.093254	0.084512	0.081013	0.080632	0.079022	0.079030
0.01		0.147739	0.098331	0.089761	0.086328	0.085955	0.084381	0.084389
0.1		0.190311	0.147216	0.140183	0.137336	0.137030	0.135768	0.135770
1	2	0.513514	0.502053	0.500960	0.500430	0.500383	0.500212	0.500220
10		1.305085	1.304799	1.304799	1.304772	1.304772	1.304770	1.304800
100		1.620690	1.627780	1.627851	1.627939	1.627942	1.627940	1.627900
1000		1.661941	1.671344	1.671489	1.671646	1.671652	1.671660	1.671600
10^5		1.666619	1.676312	1.676468	1.676635	1.676641	1.676650	1.676600
10^7		1.666666	1.676362	1.676518	1.676685	1.676691	1.676700	1.676700
10^{-7}		0.142857	0.092688	0.083926	0.080420	0.080038	0.078424	0.078423
10^{-5}		0.142862	0.092693	0.083932	0.080426	0.080044	0.078431	0.078438
0.001		0.143347	0.093254	0.084512	0.081013	0.080632	0.079023	0.079030
0.01		0.147751	0.098344	0.089775	0.086342	0.085968	0.084395	0.084402
0.1		0.191441	0.148481	0.141474	0.138636	0.138332	0.137074	0.137080
1	50	0.595773	0.588092	0.587389	0.587039	0.587009	0.586898	0.586900
10		2.842520	2.895365	2.895347	2.894793	2.894785	2.894780	2.894800
100		5.500000	6.978402	7.189395	7.262994	7.270545	7.286740	7.287200
1000		6.084922	8.384497	8.897360	9.113386	9.137249	9.224800	9.225600
10^5		6.157156	8.579661	9.149738	9.396639	9.424103	9.532260	9.533100
10^7		6.157887	8.581664	9.152350	9.399586	9.427089	9.535470	9.536300

* Table 1, 6th order formula, at [25]

** Table 3, at [22]

† Table 1, at [33]

4 | PROPERTY GAIN

In [13] an Ad-hoc homogenization model was developed to analyze the role of aggregation processes and interfacial thermal resistance on the effective thermal conductivity of nanofluids and nanocomposites. Gain has also been reported for multiscale fibrous and particulate composites [16,17,18] considering perfect contact. In the case of laminates, it was also reported [12,20] taking into account imperfect contact.

Given $K^{(m)}$, $K^{(i)}$ the thermal conductivities of the matrix and inclusions, lets denote by $\hat{K}_{CH}$, $\hat{K}_{RH}$ the effective coefficient of the whole medium obtained via conventional and reiterated homogenization. For our isotropic medium case we can write them in terms of their scalar equivalents:

$$K^{(m)} = k^{(m)} I,\ K^{(i)} = k^{(i)} I,$$
$$\hat{K}_{CH} = \hat{k}_{CH} I,\ \hat{K}_{RH} = \hat{k}_{CH} I,$$

where I is the identity matrix.

These quantities will depend on the volume fraction of inclusions (ϕ), the phase conductivity ratio ($\rho = k^{(i)}/k^{(m)}$), the geometry and the thermal barrier (characterized by β). The geometry is characterized by the shape of the inclusions and, for $\hat{k}_{RH}$ will also depend on the shape of the clusters and the aggregation parameter (α), previously discussed in 1.1.

Both, $\hat{k}_{CH}$ and $\hat{k}_{RH}$ can be calculated by means of the formulas obtained in Section 3.2, or other means. We obtain $\hat{k}_{CH}$ by direct application of the fifth order formula (52), and $\hat{k}_{RH}$ applying the same formula twice: first in (10) to obtain the intermediate effective coefficient (13) and finally in (11) to obtain the global effective coefficient (12). Notice that, from (41)-(42) they have the isotropy property and only one coefficient should be calculated in each step.

For comparison we consider the cases where the volume fraction ϕ of the inclusions are the same and the complexity of the second media is characterized by the aggregation parameter α. We are particularly interested in the benefits or inconvenience

TABLE 4 Comparison of effective conductivities for volume fractions near percolation ($\phi = 0.78$) with different approximations[23]

Bi	ρ	Eq.(45)	Eq.(48)	Eq.(49)	Eq.(51)	[23]*
0	6	0.1236	0.0641	0.0487	0.0405	0.0279
12		2.2787	2.3029	2.3029	2.3026	2.3026
40		3.0176	3.1835	3.1912	3.1942	3.1946
240		3.4214	3.7491	3.7843	3.8001	3.8068
800		3.4872	3.8488	3.8925	3.9129	3.9233
$2 \cdot 10^{12}$		3.5161	3.8935	3.9415	3.9643	3.9771
0	400	0.1236	0.0641	0.0487	0.0405	0.0279
12		3.4872	3.6452	3.6462	3.6455	3.6454
40		5.7156	7.3012	7.5026	7.5662	7.5823
240		7.4488	12.5760	14.7625	16.0557	17.3740
800		7.7811	14.0994	17.5498	20.0453	24.2400
$2 \cdot 10^{12}$		7.9329	14.8821	19.1605	22.6171	31.0040

*Table 3, $N_0 = 20$, at[23]

of considering two micro-scales (reiterated homogenization) against only one micro-scale (conventional homogenization). For this purpose we define a *gain function* as in[16] in the form:

$$k_{gain}(\alpha, \phi, \rho, \beta) \equiv \frac{\hat{k}_{RH}(\alpha, \phi, \rho, \beta)}{\hat{k}_{CH}(\phi, \rho, \beta)}. \tag{55}$$

We will analyze the effect of the thermal barrier at the interface for two-phase media which inclusions have higher conductivity than the matrix ($\rho = 500$).

For greater Biot numbers (better contact) the gain continues its tendency to grow for low concentrations and decrease with high concentrations (Figure 4). This gains, as in the perfect contact, have a maximum up to 9% for $\phi \in (0.5, 0.6)$ and $\alpha \approx 0.6$.

Figure 5 shows the influence of aggregation in the property gain in the case of perfect contact. The gain tends to grow with the concentration and for the higher concentrations, the gain oscillates around the obtained for $\phi = 0.6$ and starts to decrease reporting loss near the maximum (percolation).

For smaller Biot numbers (worst contact) the behavior is the opposite: the gain decreases for small concentrations with certain loss and starts to grow for higher ones (Figure 6). The concentration value where this change of behavior happens decreases when the Biot number decreases, reporting gains for each fixed small Biot at higher concentrations. On the other hand, the maximum gain increases when the Biot number decreases, being higher than 25% in the case of $Bi \to 0$, which represents decoupling of the phases. Independence of ρ for no gain/loss value also occurs in this case.

It is physically expected that the gain should increase as the Biot number decreases and this behavior is reflected in our results. In fact, the three-scale geometric arrangement is better conductive than the associated two-scale counterpart. Thus, the better conductive three-scale geometric arrangement will be relatively more important as the interfacial thermal barrier increases.

5 | CONCLUDING REMARKS

In the present work, the reiterated homogenization method was applied to investigate the macroscopic behavior of fibrous composites with aggregation. Although the model and procedures are very general, due to the limitation of analytical procedures employed, for application purposes, we restrict our work to parallel isotropic long fibers with two microstructural levels. A thermal barrier was considered assuming imperfect spring-type contact condition at the interface[24].

The partial differential equations derived from reiterated homogenization method (RH) were solved via an analytical method, following the Rayleigh method. We derive five types of explicit analytical formulas for the effective thermal coefficient with different approximation orders (Eq. (45),(48),(49),(51),(52)).

These formulas are expressed in the style of those reported by[25] for perfect contact in a three-phase conductive problem, establishing an equivalence relationship between both models. The comparison with results in the literature, including the finite

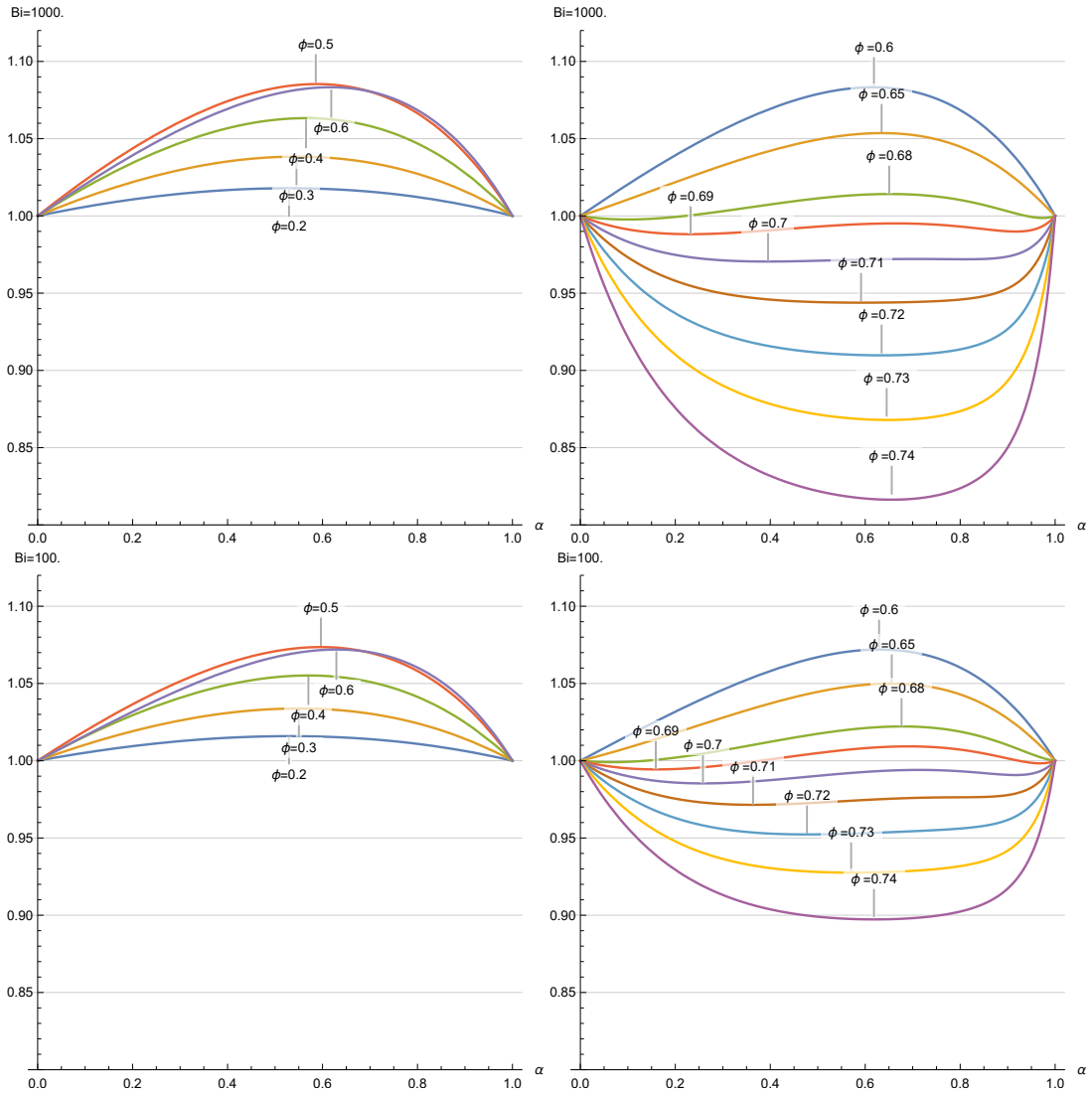

FIGURE 4 Gain for $\rho = 500$ as a function of the agregation for different concentrations and high Biot numbers $Bi \in \{10^3; 10^2\}$).

element method[33], showed an improvement of the accuracy as truncation order increase. In particular, for small concentrations, the obtained Laurent series expansion is a generalization of the results in[29] (Eq.(54)).

The two micro-structural levels analysis in[16] is generalized to the case of imperfect interfacial contact. The results reveal the role of aggregation processes and imperfect contact in thermal conductivity. In fact, we can identify the ranges of problem parameters in which the arrangement of the inclusions in three-scales leads to gain/loss relative to the conventional two-scales arrangement. It has been found that the values of the gain are highly dependent on Biot numbers, with attained maximums that go from 9% when $Bi \to \infty$ (perfect contact) to beyond 25% when $Bi \to 0$ (decoupling). Besides, while[16] considered low volume fraction, our method is also feasible in high volume fraction cases.

APPENDIX: COMPARISON WITH THREE-PHASE MEDIUM

In the literature, there are different ways of modeling imperfect contact. So far it has been considered the imperfection as a surface with certain effect that separates two phases, one representing the matrix and the other formed by the inclusions. Another model can be based on considering a three-phase medium, the ones mentioned and a third that separates both, with its own

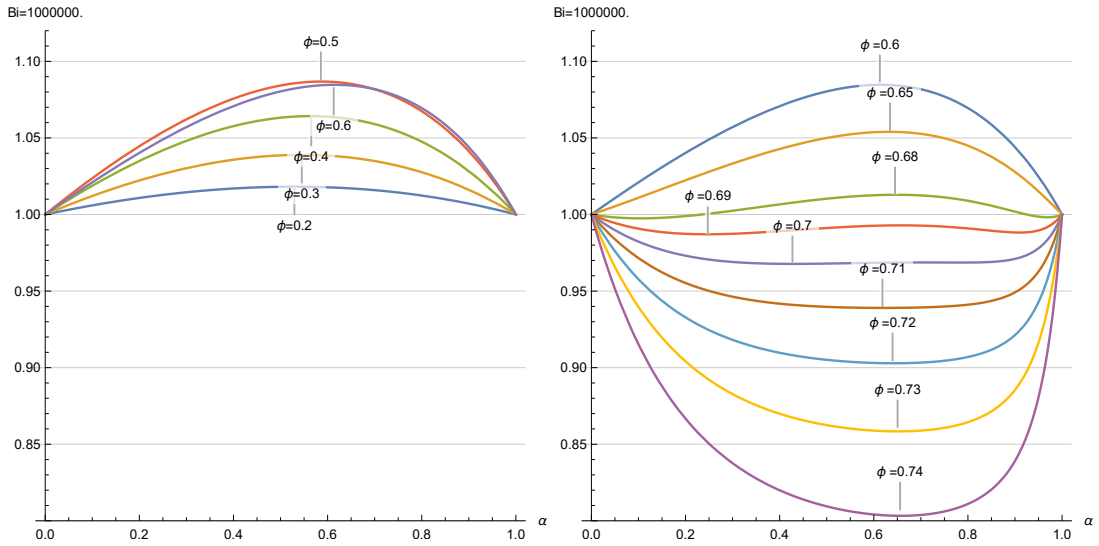

FIGURE 5 Gain for $\rho = 500$ as a function of the agregation for different concentrations. In this case the perfect contact ($Bi \to \infty$) is computed using the by aproximation $Bi = 10^6$.

characteristics and properties. In this way, when the thickness of the intermediate layer is very thin, both models should be equivalent (Figure 7).

For this three-phase model, there are two main difficulties: From the theoretical point of view, the difficulty is to guarantee the equivalence of both in the limit (existence of said limit, that the problems are well-posed, etc.). From a practical point of view, the numerical methods some times not converge to the correct value when the dimensions of the layer are very small (due to discretization, aliasing, and other numerical artifacts).

In this section, we will compare the analytical results of[25] for a three-phase model with our proposal. In this way, for small thicknesses, we can validate our results and look for conditions that guarantee the equivalence of both models, at least in the limiting cases, when the thickness tends to zero.

We will denote by

$$\kappa(y) = \begin{cases} \kappa^{(m)}, & y \in Y^{(m)} \quad \text{(matrix)}, \\ \kappa^{(\Gamma)}, & y \in Y^{(\Gamma)} \quad \text{(interface)}, \\ \kappa^{(i)}, & y \in Y^{(i)} \quad \text{(inclusion)}, \end{cases}$$

and by

$$r_o = r + \frac{\delta}{2}, \qquad r_i = r - \frac{\delta}{2}.$$

Hypothesis: The following developments will be carried out under the assumption that there is a certain normalization constant $C(r)$ such that, for the models presented, the following limit exists:

$$\lim_{\delta \to 0} \frac{\kappa^{\Gamma}}{\delta \beta} = C(r). \tag{56}$$

In[25] we obtain approximations of the effective property of the form

$$F_{\text{cond}} \equiv \frac{\hat{\kappa}}{\kappa^{(m)}} = \frac{1 - \phi v_1 - terms}{1 + \phi v_1 - terms} = 1 - \frac{2\phi v_1}{1 + \phi v_1 - terms}. \tag{57}$$

where *terms*is a weighted sum of terms of ϕ whose coefficients are calculated using the following formulas:

$$v_k = \frac{\chi_o + \chi_i \left(\frac{r_i}{r_o}\right)^{2k}}{1 + \chi_o \chi_i \left(\frac{r_i}{r_o}\right)^{2k}}, \tag{58}$$

where

$$\chi_o = \frac{\kappa^{(m)} - \kappa^{(\Gamma)}}{\kappa^{(m)} + \kappa^{(\Gamma)}}, \qquad \chi_i = \frac{\kappa^{(\Gamma)} - \kappa^{(i)}}{\kappa^{(\Gamma)} + \kappa^{(i)}}.$$

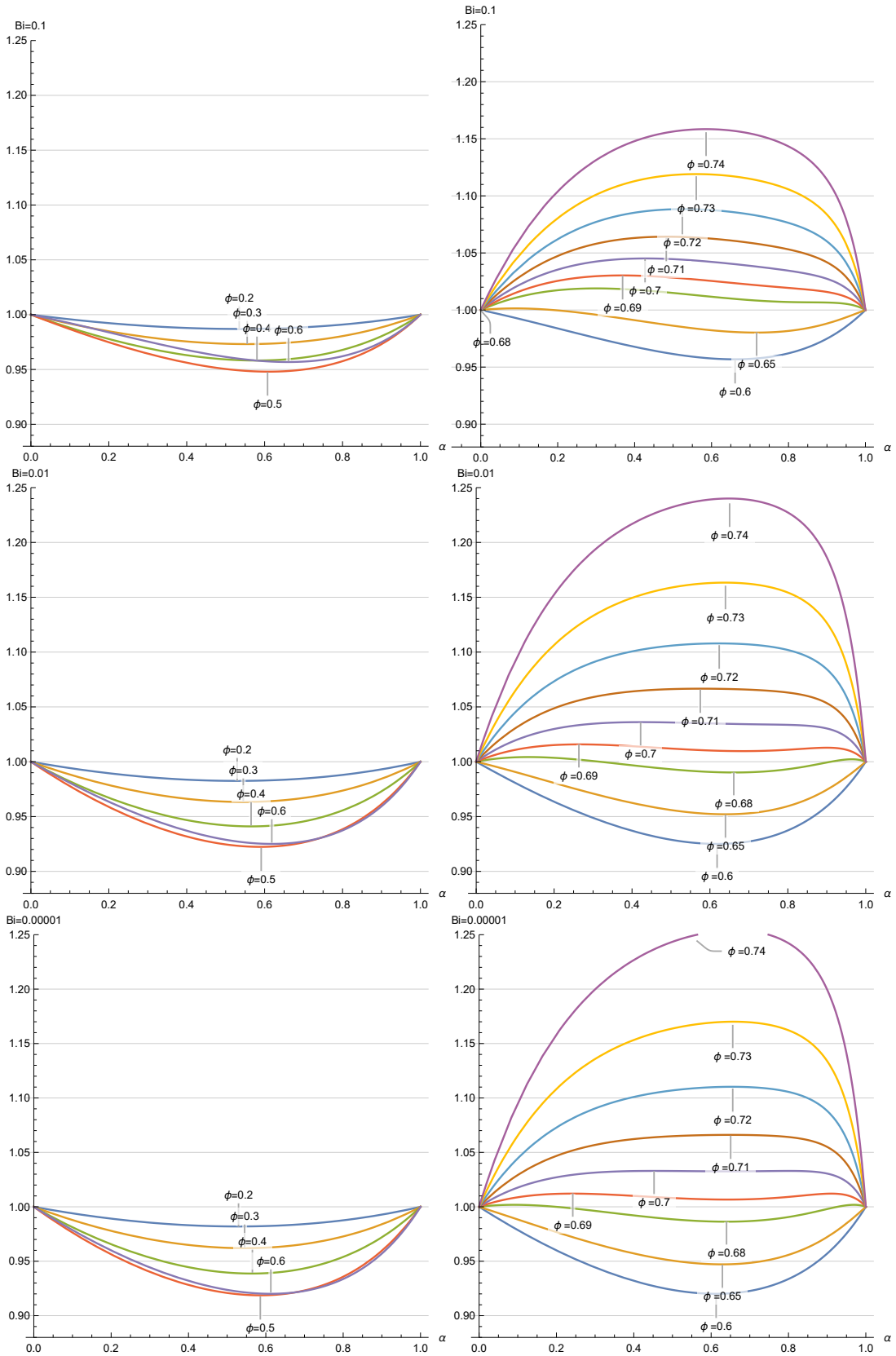

FIGURE 6 Gain for $\rho = 500$ as a function of the agregation for different concentrations and small Biots numbers ($Bi \in \{10^{-1}; 10^{-2}; 10^{-5}\}$).

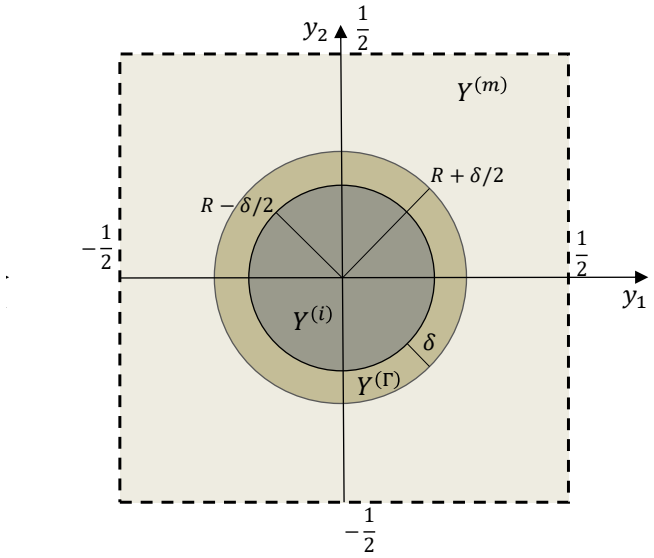

FIGURE 7 Cross section of an equivalent three-phase medium.

In the table 5 we present the explicit formulas for *terms*.

Our intention is to find the relationship between υ_k and β_k from (37) and (58), as long as $\delta << 1$.

Let's rewrite

$$\begin{aligned}\upsilon_k &= \frac{(\kappa^{(m)}-\kappa^{(\Gamma)})(\kappa^{(\Gamma)}+\kappa^{(i)})+(\kappa^{(m)}+\kappa^{(\Gamma)})(\kappa^{(\Gamma)}-\kappa^{(i)})\left(\frac{r_i}{r_o}\right)^{2k}}{(\kappa^{(m)}+\kappa^{(\Gamma)})(\kappa^{(\Gamma)}+\kappa^{(i)})+(\kappa^{(m)}-\kappa^{(\Gamma)})(\kappa^{(\Gamma)}-\kappa^{(i)})\left(\frac{r_i}{r_o}\right)^{2k}} \\ &= \frac{2(1-\rho)\kappa^{(\Gamma)}+\kappa^{(i)}\left(1-\left(\frac{r_i}{r_o}\right)^{2k}\right)-\kappa^{(\Gamma)}A_k^-}{2(1+\rho)\kappa^{(\Gamma)}+\kappa^{(i)}\left(1-\left(\frac{r_i}{r_o}\right)^{2k}\right)-\kappa^{(\Gamma)}A_k^+},\end{aligned}$$

where

$$\begin{aligned}A_n^- &= \left(1-\frac{\kappa^{(i)}-\kappa^{(\Gamma)}}{\kappa^{(m)}}\right)\left(1-\left(\frac{r_i}{r_o}\right)^{2n}\right), \\ A_n^+ &= \left(1+\frac{\kappa^{(i)}-\kappa^{(\Gamma)}}{\kappa^{(m)}}\right)\left(1-\left(\frac{r_i}{r_o}\right)^{2n}\right).\end{aligned}$$

In this way the limits

$$\lim_{\delta\to 0}\upsilon_k = \frac{(1-\rho)rC(r)\beta+k\kappa^{(i)}}{(1+\rho)rC(r)\beta+k\kappa^{(i)}} \tag{59}$$

are obtained.

This means that in (56), using the normalization

$$\kappa^{(\Gamma)} = \frac{\delta\beta}{r} \tag{60}$$

it is possible to establish a parallelism between our model and the three-phase model proposed by[25] being

$$\beta_k = \lim_{\delta\to 0}\upsilon_k.$$

This normalization (60) also coincides with the proposals in[26,27,22]. In other words, given a sufficiently small thickness δ and if we know β in our imperfect contact model, it is possible to calculate a $\kappa^{(\Gamma)} = \delta\beta/r$, for which the three-phase model is equivalent, and vice versa (find β knowing $\kappa^{(\Gamma)}$).

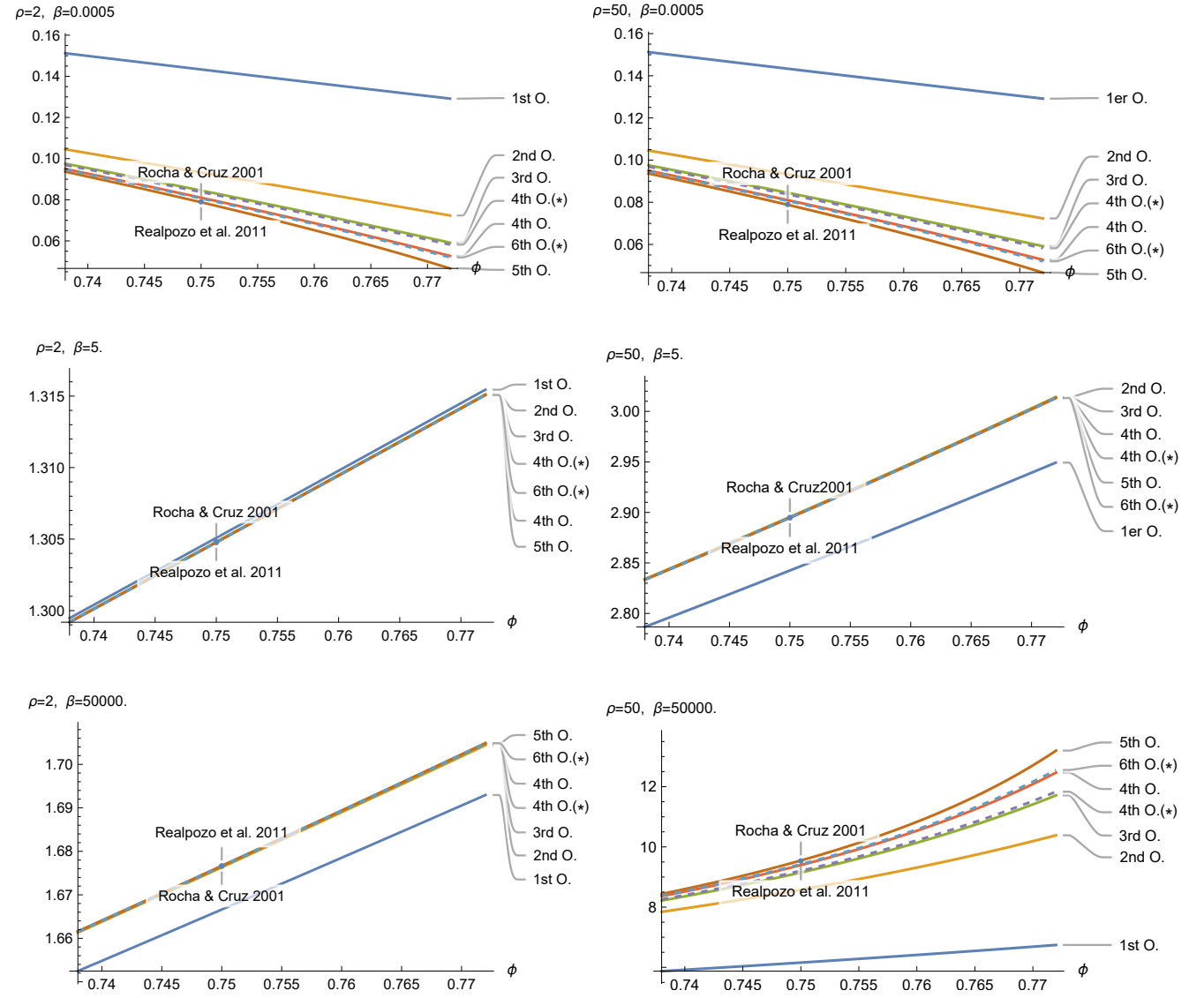

FIGURE 8 Comparison of effective conductivities estimates for high volume fractions. For the computation of the dashed curves (marked with *), the formulas from [25] were used instead of ours.

From the numerical point of view, the approximations obtained by us in the section 3.3 coincide reasonably with the results presented by [25]. In fact the accompanying terms in (57) coincide for the first and second truncation of the system (equations (45) and (48) respectively). For third-order truncation, some differences appear between the two approximations, since while [25] proposes the same approximation of the previous order, in our case, it was obtained (49). The fourth- and fifth-order differs even more and an exact equivalence cannot be established between its results and ours. In the figure 8 some values from the literature are also shown together with the approximations in a close range. Table 5 presents a summary of this comparison between the results in [25] and ours.

TABLE 5 Comparison between[25] (square cell) and the present work.

Trunc. Order	Eq.(45),(48)-(52) $\frac{\hat{\kappa}_{11}}{\kappa^{(m)}} = \frac{1-\phi\beta_1-\tau}{1+\phi\beta_1-\tau}$	Manteufel-Todreas[25] $\frac{\hat{\kappa}_{11}}{\kappa^{(m)}} = \frac{1-\phi v_1-\tau}{1+\phi v_1-\tau}$	Coefficients and auxiliary functions
1º	$\tau = 0$	$\tau = 0$	
2º	$\tau = C_4\beta_1\beta_3\phi^4$	$\tau = C_4 v_1 v_3 \phi^4$	$C_4 = 3S_4^2\pi^{-4} \approx 0.305827833$
3º	$\tau = C_4\beta_1\beta_3\phi^4/\Delta_1(\phi)$		$\Delta_1(\phi) = 1 - b_8\beta_3\beta_5\phi^8$ $b_8 = 735S_8^2\pi^{-8} \approx 1.40295995$
4º	$\tau = C_4\beta_1\beta_3\phi^4/\Delta_2(\phi) + C_8\beta_1\beta_7\phi^8\frac{\Delta_1'(\phi)}{\Delta_2(\phi)}$	$\tau = C_4 v_1 v_3 \phi^4/D_1(\phi) + C_8 v_1 v_7 \phi^8$	$C_8 = 7S_8^2\pi^{-8} \approx 0.013361523$ $D_1(\phi) = 1 - b_8 v_3 v_5 \phi^8$ $\Delta_2(\phi) = 1 - \frac{5041}{13^2} b_8\beta_3\beta_5\phi^8$ $\Delta_1'(\phi) = \Delta_1(\phi) - b_{12}\beta_5\beta_7\phi^{12}$ $b_{12} = 152460S_{12}^2\pi^{-12} \approx 2.55915216$
5º	$\tau = C_4\beta_1\beta_3\phi^4\frac{\Delta_0(\phi)}{\Delta_3(\phi)} + C_8\beta_1\beta_7\phi^8\frac{\Delta_2'(\phi)}{\Delta_3(\phi)}$		$\Delta_0(\phi) = 1 - b_{12}\beta_5\beta_7\phi^{12} - b_{16}\beta_7\beta_9\phi^{16}$ $\Delta_3(\phi) = \Delta_2(\phi) - b_{12}'\beta_3\beta_9\phi^{12} - b_{16}\beta_7\beta_9\phi^{16} - C_{24}\beta_3\beta_5\beta_7\beta_9\phi^{24}$ $\Delta_2'(\phi) = \Delta_1'(\phi) + \frac{168}{13} b_8\beta_3\beta_5\phi^8 + \frac{1001}{17} b_{12}'\beta_3\beta_9\phi^{12}$ $b_{12}' = \frac{5}{84} b_{12} \approx 0.15233049$ $b_{16} = 32207175S_{16}^2\pi^{-16} \approx 5.76867559$ $C_{24} = 2858625(22S_{12}^2 - 91S_{16}S_8)^2\pi^{-24} \approx 4.93057350$
6º&7º		$\tau = C_4 v_1 v_3 \phi^4/D_2(\phi) + C_8 v_1 v_7 \phi^8 + C_{12}(v_1)^2\phi^{12} + C_{16}v_1 v_3 v_5 v_7 \phi^{16}/D_3(\phi) + C_{20}v_1 v_5 (v_7)^2\phi^{20}/D_0(\phi) + C_{28}v_1 v_3 (v_5)^2 (v_7)^2\phi^{28}/D_4(\phi)$	$C_{12} \approx 0.000184643; C_{16} \approx 0.242252;$ $C_{20} \approx 0.0341942; C_{28} \approx 0.0479731;$ $D_0(\phi) = 1 - b_{12}v_5 v_7\phi^{12},$ $D_2(\phi) = 1 - b_8 v_3 v_5 \phi^8/D_0(\phi) - b_{12}' v_3 v_9 \phi^{12}$ $D_3(\phi) = 1 - b_8 v_3 v_5 \phi^8/D_0(\phi) - \left[b_{12}v_5 v_7 + b_{12}' v_3 v_9\right]\phi^{12} + b_{20}v_3 \left(v_5\right)^2 v_7 \phi^{20}/D_0(\phi) + b_{24}v_3 v_5 v_7 v_9 \phi^{24}$ $D_4(\phi) = 1 - b_8 v_3 v_5 \phi^8/D_0(\phi) - [2b_{12}v_5 v_7 + b_{12}' v_3 v_9]\phi^{12} + 2b_{20}v_3 (v_5)^2 v_7 \phi^{20}/D_0(\phi) + [2b_{24}v_3 v_5 v_7 v_9 + b_{24}'(v_5)^2 (v_7)^2]\phi^{24} - b_{32}v_3 (v_5)^3 (v_7)^2 \phi^{32}/D_0(\phi) - b_{36}v_3 (v_5)^2 (v_7)^2 v_9 \phi^{36}$
Where: $b_{20} = 3.59039, b_{24} = 0.389837, b_{24}' = \frac{84}{5} b_{24}, b_{32} = 9.18835, b_{36} = 0.997652$			

ACKNOWLEDGEMENTS

E. Iglesias-Rodríguez would like to thank CONACYT for support his PhD studies at UNAM. Prof. M. E. Cruz is grateful to CNPq-Brazilian Council for Development of Science and Technology for Grant PQ-305089-2020/0. Project PAPIIT DGAPA UNAM IN101822 is also recognized.

References

1. Greco A.. Numerical simulation and mathematical modeling of 2D multi-scale diffusion in lamellar nanocomposite. *Computational Materials Science.* 2014;90:203–209.

2. Mortazavi Bohayra, Benzerara Olivier, Meyer Hendrik, Bardon Julien, Ahzi Said. Combined molecular dynamics-finite element multiscale modeling of thermal conduction in graphene epoxy nanocomposites. *Carbon.* 2013;60:356–365.

3. Shin Hyunseong, Yang Seunghwa, Chang Seongmin, Yu Suyoung, Cho Maenghyo. Multiscale homogenization modeling for thermal transport properties of polymer nanocomposites with Kapitza thermal resistance. 2013;.

4. Díaz Ariel R., Flores Erick I. Saavedra, Yanez Sergio J., Vasco Diego A., Pina Juan C., Guzmán Carlos F.. Multiscale modeling of the thermal conductivity of wood and its application to cross-laminated timber. *International Journal of Thermal Sciences.* 2019;144:79–92.

5. Clancy T.C., Frankland S.J.V., Hinkley J.A., Gates T.S.. Multiscale modeling of thermal conductivity of polymer/carbon nanocomposites. *International Journal of Thermal Sciences.* 2010;49(9):1555–1560.

6. Angayarkanni S. A., Philip John. Review on Thermal Properties of Nanofluids: Recent Developments. *Advances in Colloid and Interface Science.* 2015;225:146–176.

7. Vatani Ashkan, Woodfield Peter Lloyd, Dao Dzung Viet. A survey of practical equations for prediction of effective thermal conductivity of spherical-particle nanofluids. *Journal of Molecular Liquids.* 2015;211:712–733.

8. Jin Jae Sik, Lee Joon Sik. Effects of Aggregated Sphere Distribution and Percolation on Thermal Conduction of Nanofluids. *Journal of Thermophysics and Heat Transfer.* 2013;27(1):173–178.

9. Wang J. J., Zheng R. T., Gao J. W., Chen G.. Heat conduction mechanisms in nanofluids and suspensions. *Nano Today.* 2012;7:124–136.

10. Hassaan Amr M.. An investigation for the performance of the using of nanofluids in shell and tube heat exchanger. *International Journal of Thermal Sciences.* 2022;177:107569.

11. López-Ruiz Gabriela, Bravo-Castillero Julián, Brenner Renald, et al. Variational bounds in composites with nonuniform interfacial thermal resistance. *Applied Mathematical Modelling.* 2015;39:7266–7276.

12. Álvarez-Borges F. E., Bravo-Castillero J., Cruz M. E., et al. Reiterated homogenization of a laminate with imperfect contact: gain-enhancement of effective properties. *Applied Mathematics and Mechanics.* 2018;39(8):1119–1146.

13. Evans William, Prasher Ravi, Fish Jacob, Meakin Paul, Phelan Patrick, Keblinski Pawel. Effect of aggregation and interfacial thermal resistance on thermal conductivity of nanocomposites and colloidal nanofluids. *International Journal of Heat and Mass Transfer.* 2008;51:1431–1438.

14. Bensoussan Alain, Lions Jacques-Louis, Papanicolau George. *Asymptotic Analysis for Periodic Structures*. Studies in Mathematics and its ApplicationsNorth-Holland Publishing Company; 1978.

15. Iglesias-Rodríguez Ernesto, Cruz Manuel E., Bravo-Castillero Julián. Reiterated homogenization applied to heat conduction in heterogeneous media with multiple spatial scales and perfect thermal contact between the phases. *Journal of the Brazilian Society of Mechanical Sciences and Engineering.* 2016;38:1333–1343.

16. Nascimento Eduardo S., Cruz Manuel E., Bravo-Castillero Julián. Calculation of the effective thermal conductivity of multiscale ordered arrays based on reiterated homogenization theory and analytical formulae. 2017;:205–216.

17. Mattos Lucas Prado, Cruz Manuel Ernani, Bravo-Castillero Julián. Finite element computation of the effective thermal conductivity of two-dimensional multi-scale heterogeneous media. *Engineering Computations.* 2018;35(5):2107–2123.

18. Dong Hao, Zheng Xiaojing, Cui Junzhi, Nie Yufeng, Yang Zhiqiang, Yang Zihao. High-order three-scale computational method for dynamic thermo-mechanical problems of composite structures with multiple spatial scales. *International Journal of Solids and Structures.* 2019;169:95–121.

19. Ma Qiang, Ye Shuyu, Cui Junzhi, Yang Zhiqiang, Jiang Xue, Li Zhihui. Two-scale and three-scale asymptotic computations of the Neumann-type eigenvalue problems for hierarchically perforated materials. 2021;92:565–593.

20. Iglesias Rodríguez Ernesto, Bravo-Castillero Julián, Cruz Manuel E., Pérez-Fernández Leslie D., Sabina Federico J.. Reiterated homogenization applied to nanofluids with an interfacial thermal resistance. *International Journal for Multiscale Computational Engineering.* 2020;18:361–384.

21. Rodríguez-Ramos R., Sabina F. J., Guinovart-Díaz R., Bravo-Castillero J.. Closed-form expressions for the effective coefficients of a fiber-reinforced composite with transversely isotropic constituents – I. Elastic and square symmetry. *Mechanics of Materials.* 2001;(33):223–235.

22. López-Realpozo Juan C., Rodríguez-Ramos Reinaldo, Guinovart-Díaz Raúl, Bravo-Castillero Julián, Sabina Federico J.. Transport properties in fibrous elastic rhombic composite with imperfect contact condition. *International Journal of Mechanical Sciences.* 2011;53(2):98–107.

23. Guinovart-Díaz R., Rodríguez-Ramos R., Bravo-Castillero J., López-Realpozo J. C., Sabina F. J., Sevostianov I.. Effective elastic properties of a periodic fiber reinforced composite with parallelogram-like arrangement of fibers and imperfect contact between matrix and fibers. 2013;50:2022-2032.

24. Hashin Zvi. Thin interphase/imperfect interface in conduction. 2001;89(4):2261–2267.

25. Manteufel R.D., Todreas N.E.. Analytic formulae for the effective conductivity of a square or hexagonal array of parallel tubes. *International Journal of Heat and Mass Transfer.* 1994;37(4):647–657.

26. Hashin Z.. The Spherical Inclusion With Imperfect Interface. 1991;58(2):444–449.

27. Hashin Zvi. Thin interphase/imperfect interface in elasticity with application to coated fiber composites. *Journal of the Mechanics and Physics of Solids.* 2002;50(12):2509–2537.

28. Sevostianov I., Rodriguez-Ramos R., Guinovart-Diaz R., Bravo-Castillero J., Sabina F.J.. Connections between different models describing imperfect interfaces in periodic fiber-reinforced composites. 2012;49(13):1518–1525.

29. Godin Yuri A.. The effective conductivity of a periodic lattice of circular inclusions. *Journal of Mathematical Physics.* 2012;53(6):063703.

30. Liang Jian Xun, Cai Yun Tao. Application of Advanced Carbon Fiber Composite Material in Sport Equipments. *Applied Mechanics and Materials.* 2012;217-219:63–66.

31. Keshtkar Mahboube, Mehdipour Nargess, Eslami Hossein. Thermal Conductivity of Polyamide-6,6/Carbon Nanotube Composites: Effects of Tube Diameter and Polymer Linkage between Tubes. *Polymers.* 2019;11(9):1465.

32. Rand B. *Design and Control of Structure of Advanced Carbon Materials for Enhanced Performance*. Dordrecht: Springer Netherlands; 2001.

33. Rocha Rodrigo P. A., Cruz Manuel Ernani. Computation of the Effective Conductivity of Unidirectional Fibrous Composites With an Interfacial Thermal Resistance. *Numerical Heat Transfer, Part A: Applications.* 2001;39(2):179–203.

34. López-Realpozo Juan C., Rodríguez-Ramos Reinaldo, Guinovart-Díaz Raúl, et al. Effective elastic shear stiffness of a periodic fibrous composite with non-uniform imperfect contact between the matrix and the fibers. *International Journal of Solids and Structures.* 2014;51(6):1253–1262.

35. Lienhard IV John H., Lienhard V John H.. *A heat transfer textbook*. Phlogiston Press; 3 ed.2005.

36. Allaire G., Briane M.. Multiscale convergence and reiterated homogenization. *Proceedings of the Royal Society of Edinburgh.* 1996;126A:297–142.

37. Meunier Nicolas, Van Schaftingen Jean. Periodic reiterated homogenization for elliptic functions. *Journal de mathématiques pures et appliquées.* 2005;84(12):1716–1743.

38. Cioranescu Doina, Saint-Jean Paulin Jeannine. *Homogenization of Reticulated Structures*. Applied Mathematical SciencesSpringer; 1998.

39. Brëzis Ham. *Análisis Funcional. Teoría y Aplicaciones*. Alianza Editorial S.A.; 1984.

40. Babuška Ivo. Solution of Interface Problems by Homogenization. I. *SIAM Journal on Numerical Analysis.* 1976;7(5):603–634.

41. Babuška Ivo. Solution of Interface Problems by Homogenization. II. *SIAM Journal on Numerical Analysis.* 1976;7(5):635–645.

42. Babuška Ivo. Solution of Interface Problems by Homogenization. III. *SIAM Journal on Numerical Analysis.* 1977;8(6):923–937.

43. Sanchez-Palencia Enrique Evariste. Comportements local et macroscopique dun type de milieux physiques hétérogènes. *International Journal Of Engineering Science.* 1974;12(4):331–351.

44. Sanchez-Palencia Enrique Evariste. *Non-Homogeneous Media and Vibration Theory*. Lecture Notes in PhysicsMoscú: Mir; 1984.

45. Bakhvalov N. S., Panasenko G. P.. *Homogenozation: Averaging Processes in Periodic Media*. Kluwer Academic Publishers; 1989.

46. Mitropolsky Yu. A., Lopatin A. K.. *Nonlinear Mechanics, Groups and Symmetry* Mathematics and Its Applications, vol. 319: . Kluwer Academic Publishers; 1995.

47. Allaire Grégoire. A Brief Introduction to Homogenization and Miscellaneous Applications. In: Cancès E., Labbé S., eds. *ESAIM: PROCEEDINGS*, :1–49; 2012.

48. Auriault Jean-Louis. Effective macroscopic description for heat conduction in periodic composites. *International Journal of Heat and Mass Transfer.* 1983;26(6):861–869.

49. Tartar Luc. *The General Theory of Homogenization: A Personalized Introduction* Lecture Notes of the Unione Matematica Italiana, vol. 7: . Springer; 2009.

50. Markushévich Alexei I.. *Teoría de las funciones analíticas*. Mir; 1970.

51. Bravo-Castillero J., Sabina F. J., Guinovart-Díaz R., Rodríguez-Ramos R.. Closed-form expressions for the effective coefficients of a fiber-reinforced composite with transversely isotropic constituents – II. Piezoelectric and square symmetry. *Mechanics of Materials.* 2001;33(4):237–248.

52. Yañez-Olmos David, Bravo-Castillero Julián, Ramírez-Torres Ariel, Rodríguez-Ramos Reinaldo, Sabina Federico J.. Effective Coefficients of Isotropic Complex Dielectric Composites in a Hexagonal Array. *Technische Mechanik; 39; 2; 220-228; ISSN 2199-9244.* 2019;.

53. Cruz Manuel Ernani, Ghaddar Chahid K., Patera Anthony T.. A Variational-Bound Nip-Element Method for Geometrically Stiff Problems; Application to Thermal Composites and Porous Media. *Proceedings of The Royal Society, A: Mathematical Physical And Engineering Sciences.* 1995;449(1935):93–122.

54. Bravo-Castillero J., Rodríguez-Ramos Reinaldo, Guinovart-Díaz Raúl, et al. Universal Relations and Effective Coefficients of Magneto-Electro-Elastic Perforated Structures. *The Quarterly Journal of Mechanics and Applied Mathematics.* 2012;65(1):61–85.

55. Duren Peter. The Legendre Relation for Elliptic Integrals:305–315. Springer New York 1991.

56. Guinovart-Díaz R., Rodríguez-Ramos R., López-Realpozo J. C., et al. Analysis of fibrous elastic composites with nonuniform imperfect adhesion. *Acta Mechanica.* 2015;227(1):57–73.

57. Stanley Richard. *Enumerative combinatorics*. New York: Cambridge University Press; 2012.

58. Grimaldi Ralph. *Discrete and combinatorial mathematics : an applied introduction*. Boston: Pearson Addison Wesley; 2004.

59. Hasselman D. P. H., Johnson Lloyd F.. Effective Thermal Conductivity of Composites with Interfacial Thermal Barrier Resistance. 1987;21:508-515.

60. Benveniste Y.. A new approach to the application of Mori-Tanaka's theory in composite materials. *Mechanics of Materials.* 1987;6(2):147–157.

61. Rayleigh Lord. LVI. On the influence of obstacles arranged in rectangular order upon the properties of a medium. *The London, Edinburgh, and Dublin Philosophical Magazine and Journal of Science.* 1892;34(211):481–502.

62. Jiang C.P., Xu Y.L., Cheung Y.K., Lo S.H.. A rigorous analytical method for doubly periodic cylindrical inclusions under longitudinal shear and its application. *Mechanics of Materials.* 2004;36(3):225–237.